ACS NANO

www.acsnano.org

ARTICLE

Enhanced Neutral Exciton Diffusion in Monolayer WS_2 by Exciton–Exciton Annihilation

Shiekh Zia Uddin,[#] Naoki Higashitarumizu,[#] Hyungjin Kim, Jun Yi, Xiang Zhang, Daryl Chrzan, and Ali Javey*

Cite This: https://doi.org/10.1021/acsnano.2c00956

Read Online

ACCESS | Metrics & More | Article Recommendations | Supporting Information

ABSTRACT: **Dominant recombination pathways in monolayer transition metal dichalcogenides (TMDCs) depend primarily on background carrier concentration, generation rate, and applied strain. Charged excitons formed in the presence of background carriers mainly recombine nonradiatively. Neutral excitons recombine completely radiatively at low generation rates, but experience nonradiative exciton–exciton annihilation (EEA) at high generation rates. Strain can suppress EEA, resulting in near-unity photoluminescence quantum yield (PL QY) at all exciton densities. Although exciton diffusion is the primary channel of energy transport in excitonic materials and a critical optoelectronic design consideration, the combined effects of these factors on exciton diffusion are not clearly understood. In this work, we decouple the diffusion of neutral and charged excitons with chemical counterdoping and explore the effect of strain and generation rate on exciton diffusion. According to the standard semiconductor paradigm, a shorter carrier recombination lifetime should lead to a smaller diffusion length. Surprisingly, we find that increasing generation rate shortens the exciton lifetime but increases the diffusion length in unstrained monolayers of TMDCs. When we suppress EEA by strain, both lifetime and diffusion length become independent of generation rate. During EEA one exciton nonradiatively recombines and kinetically energizes another exciton, which then diffuses fast. Our results probe concentration-dependent diffusion of pure neutral excitons by counterdoping and elucidate how strain controls exciton transport and many-body interactions in TMDC monolayers.**

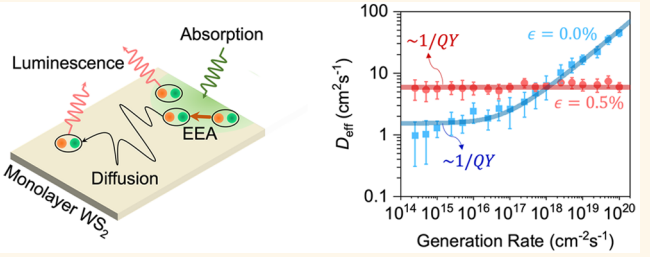

KEYWORDS: *WS_2, exciton, trion, diffusion, transport, quantum yield, strain*

INTRODUCTION

Near-unity photoluminescence (PL) quantum yield (QY) is observed in monolayers of transition metal dichalcogenides (TMDCs) at low generation rates when neutral exciton recombination is made the dominant pathway by electrostatic or chemical counterdoping.[1,2] However, neutral excitons nonradiatively recombine through exciton–exciton annihilation (EEA) at high generation rates, which drastically reduces the PL QY.[3] EEA in monolayer TMDCs can be suppressed by favorably altering the band structure through strain, resulting in near-unity PL QY at all generation rates.[4] Neutral excitons must be the dominant photocarrier in any efficient optoelectronic device since PL QY fundamentally limits the maximum attainable device efficiency. The primary mechanism of exciton transport is diffusion, and the diffusion length is an imperative design consideration for most optoelectronic applications.[5−9] While diffusion in monolayer semiconductors has been studied extensively, they are lacking on several fronts. Often the effect of background carriers is largely overlooked, producing an averaged diffusion length of both excitons and trions. Although the dependence of diffusion on exciton concentration has been noticed before,[5,8,10−12] the source of these effects was not separated into neutral and charged excitons. The effect of strain on diffusion has been reported;[13−15] however the pump dependence has been ignored. Based on our understanding of the involved photophysics of monolayer semiconductors,[4] all these factors—background carrier concentration, strain, and exciton concentration—must be simultaneously explored to get a

Received: January 27, 2022
Accepted: April 21, 2022

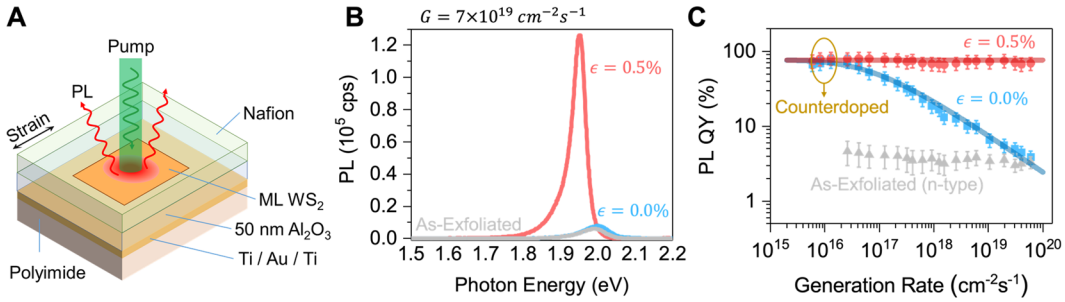

Figure 1. Strain-induced changes in photoluminescence in monolayer WS_2. (A) Schematic of the device used to explore the diffusion of excitons in monolayer WS_2. (B) PL spectra of monolayer WS_2: as-exfoliated and chemically counterdoped monolayer WS_2 at ϵ = 0%, 0.5%. (C) PL QY of monolayer WS_2 as a function of generation rate. Points, experimental data; solid lines, model.

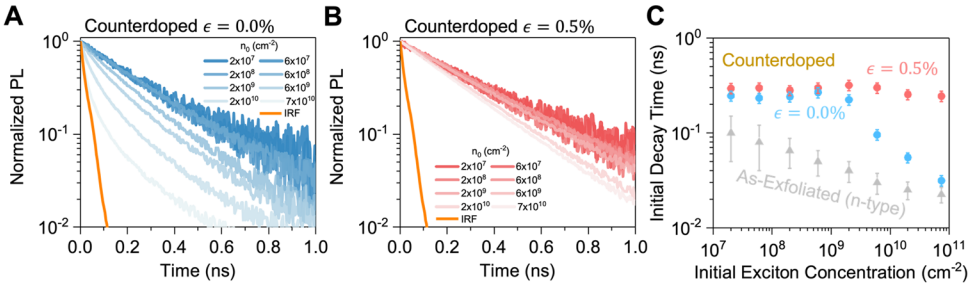

Figure 2. Time-resolved photoluminescence. (A, B) Radiative decay of chemically counterdoped monolayer WS_2 with tensile strain at different initial exciton concentrations at ϵ = 0% and 0.5%, as well as the instrument response function (IRF). (C) Effective PL lifetime as a function of initial exciton concentration: as-exfoliated and counterdoped monolayer at ϵ = 0% and 0.5%.

comprehensive understanding of the exciton diffusion process. In this work, we measure the temporal decay and spatial diffusion of pure neutral excitons under various applied strains and generation rates. We find that in an unstrained monolayer WS_2 while the exciton lifetime decreases with exciton density, the diffusion length increases with generation rate. This is highly incongruous to the conventional semiconductors, in which carrier diffusion length decreases with smaller carrier lifetime.[16] This anomalous behavior is a result of the underlying excitonic photophysics. During EEA one exciton nonradiatively transfers its energy to another exciton[17,18] and reduces both PL QY and observed lifetime. However, the energized hot excitons produced by EEA have large center-of-mass kinetic energy that thermalizes while undergoing rapid diffusion. Therefore, the average diffusion length increases with the generation rate when EEA is active. But diffusion is dominated by cold excitons when strain suppresses the EEA process, and both exciton lifetime and diffusion length become independent of generation rate. Our EEA-enhanced diffusion model considers the population of hot and cold excitons and predicts an inversely proportional relationship between exciton diffusion coefficient and PL QY, which is observed in our experiments. Strain now provides another knob to control exciton diffusion in monolayer semiconductors, along with electrostatic or chemical doping. Increased diffusion with a pump has also been observed in other excitonic semiconductors;[18,19] however our results concentrate solely on neutral excitons and establish EEA as the primary reason behind this observed enhancement. These findings uncover EEA-enhanced exciton diffusion in monolayer TMDCs and enable further engineering of neutral exciton transport in monolayer semiconductors through strain.

RESULTS AND DISCUSSION

Figure 1A shows a schematic of the device used to explore the diffusion of neutral excitons in monolayer WS_2. We used a 1.5 mm thick polyimide substrate as the strain platform for its flexibility and thermal stability, on which 10 nm titanium, 100 nm gold, and 10 nm titanium films were sequentially deposited. A 50 nm thick Al_2O_3 gate oxide was deposited on top of the metal mirror through an atomic layer deposition process. Exfoliated monolayer WS_2 was dry-transferred onto the Al_2O_3 gate oxide. As-exfoliated WS_2 is known to be n-type due to native sulfur vacancies, which generates negative trions resulting in large nonradiative recombination.[2] There is a large sample-to-sample variation in the exact doping concentration in as-exfoliated monolayers, as the exact doping concentration of a sample depends on the bulk material source, growth/exfoliation technique and environment, substrate/dielectric environment, contaminants, and impurities.[20] Such variations are often translated into fluctuations in various physical parameters measured by electrical or optical characterization.[21,22] Measured diffusion of as-exfoliated WS_2 is convoluted by coexisting neutral and charged excitons (trions), and signatures of both neutral excitons and trions are often observed together in as-exfoliated samples to a varying degree. It is therefore paramount to untangle the diffusion of neutral excitons and trions to fully understand the underlying photophysics and energy transfer. Electrostatic and chemically counterdoping can compensate for the background electron concentration and suppress the nonradiative recombination. As a hole dopant, Nafion was spin-coated on top of the monolayer to counterdope and move the Fermi level to the middle of the bandgap.[3] Calibrated PL measurements were performed to quantitatively extract the QY as a function of generation rate and strain (Materials and Methods). Figure 1B shows PL spectra of as-exfoliated and counterdoped WS_2 flakes under

https://doi.org/10.1021/acsnano.2c00956
ACS Nano XXXX, XXX, XXX−XXX

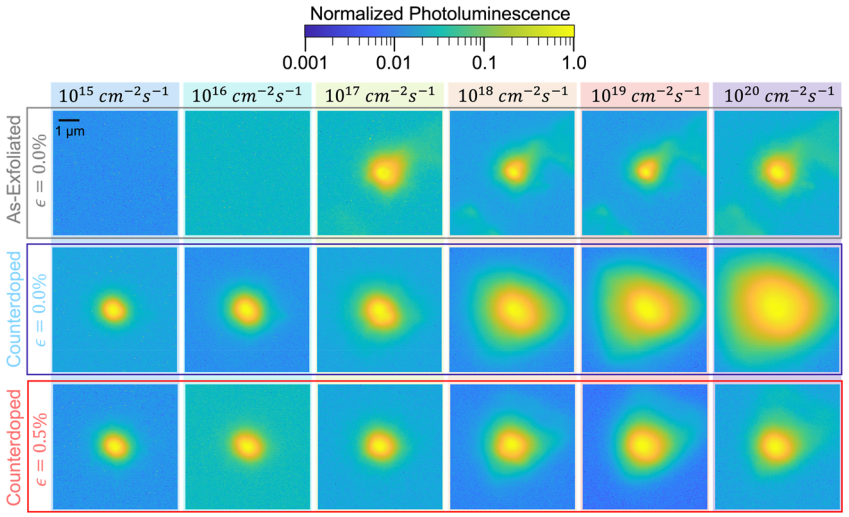

Figure 3. Neutral exciton diffusion. PL images of as-exfoliated and counterdoped monolayer WS_2 with tensile strain at ϵ = 0% and 0.5% excited by a CW laser focused on a diffraction-limited spot at different generation rates G.

different uniaxial tensile strains at a generation rate of $G = 7.0 \times 10^{19}$ cm^{-2} s^{-1}. At this high generation rate, PL intensity does not change significantly after Nafion treatment. But when 0.5% uniaxial tensile strain is applied, PL intensity increases by more than an order of magnitude. Figure 1C shows PL QY as a function of generation rate (G) for as-exfoliated and counterdoped monolayer with a different strain. Although PL QY decreases at the high generation rate for the counterdoped unstrained sample, a constant PL QY of ~73% on average was observed at all generation rates for the strained sample owing to suppressed EEA.[3]

Time-resolved (TR) PL measurements were performed on the unstrained and strained samples to investigate the effect of strain on the temporal decay of excitons. Figure 2 (A and B) shows TR PL of counterdoped monolayer WS_2 under different initial exciton concentrations at different strains of ϵ = 0% and 0.5%, respectively. We note that the unstrained sample shows an initial fast decay and then a slow decay tail, which is indicative of a density-dependent recombination channel previously attributed to EEA.[23,24] However, the strained sample shows a monoexponential decay, indicating only one recombination channel is dominant. The extracted initial decay time or lifetime for as-exfoliated and counterdoped samples is shown in Figure 2C. The trend in lifetime with initial exciton density is consistent with PL QY changes with generation rate. The lifetime of the unstrained sample shows a decrease at high initial concentration from EEA, whereas for the 0.5% strained sample it is independent of initial exciton concentrations, indicating suppression of EEA. The detailed mechanism of EEA suppression by strain is discussed in ref 4.

PL imaging is an effective tool for probing steady-state exciton diffusion in two dimensions. PL images of a WS_2 monolayer excited by a diffraction-limited 514.5 nm continuous-wave laser at different generation rate and strain are obtained to explore steady-state exciton propagation. Figure 3 shows PL images of as-exfoliated and counterdopoed monolayer WS_2 under different generation rates at tensile strains of ϵ = 0% and 0.5%. The strained monolayer shows a shorter spread compared to the unstrained monolayer. To further investigate, we first define the mean squared radius as

$$w^2 = \frac{\int \mathrm{rdr}\, \mathrm{d}\theta r^2\, I(r,\theta)}{\int \mathrm{rdr}\, \mathrm{d}\theta\, I(r,\theta)} \quad (1)$$

where $I(r, \theta)$ is the steady-state PL intensity, (r, θ) is the radial coordinate, and the integrations are limited to the area of the monolayer. The steady-state effective diffusion length (L_D) is then defined as the mean-square radius of the diffusion map deconvoluted by the laser spot size.[25] We show the measured diffusion length as a function of generation rate and strain in Figure 4A. For as-exfoliated monolayer WS_2, we observe a diffusion length of ~200 nm, consistent with previously reported values.[5,8] In the unstrained counterdoped WS_2, the

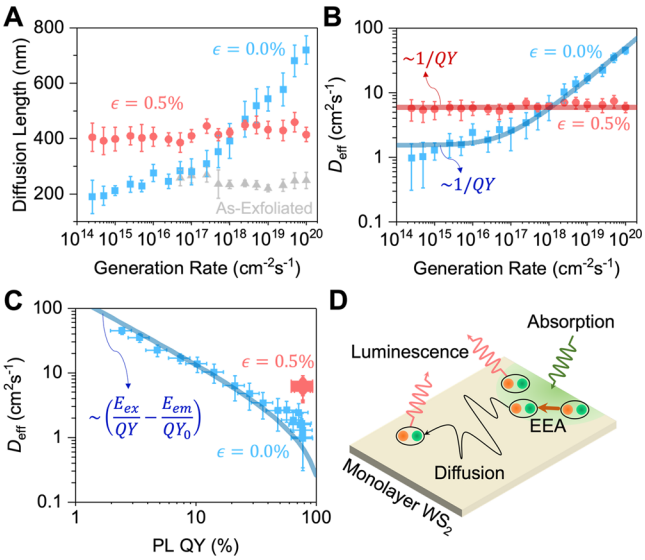

Figure 4. Exciton−exciton annihilation enhanced diffusion. (A) Diffusion length of neutral excitons in monolayer WS_2 at different generation rates and strains. (B) Effective diffusion coefficient D_{eff} *versus* generation rate for monolayer WS_2 with different strains at ϵ = 0% and 0.5%. (C) Inversely proportional relationship between D_{eff} and PL QY, which can be switched by strain. (D) Annihilation of an exciton provides additional kinetic energy to another nearby exciton to traverse further and then emit light, resulting in a large diffusion pattern.

https://doi.org/10.1021/acsnano.2c00956
ACS Nano XXXX, XXX, XXX−XXX

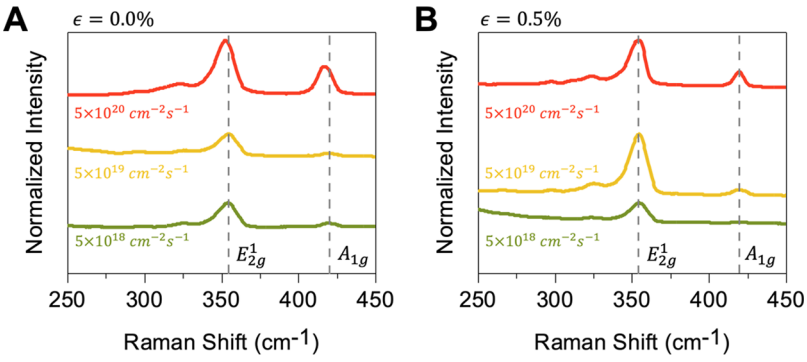

Figure 5. Raman spectra of monolayer WS_2. (A, B) Generation rate dependent Raman spectra of monolayer WS_2 with variant uniaxial strains of ϵ = 0% and 0.5%.

diffusion length increases monotonically with generation rate from $G \approx 10^{17}$ cm^{-2} s^{-1}. We emphasize that, although such an increase has been observed before,[5,10−12] our result reflects the diffusion of purely neutral excitons as we have employed chemical counterdoping, whereas previous results represent convoluted diffusion of both neutral and charged excitons (trions) that coexist at room temperature due to natural background doping. The diffusion length in a counterdoped, 0.5% strained WS_2 monolayer is ∼2 times higher than that of an unstrained monolayer at low generation rates.[15] Moreover, the diffusion length is independent of generation rate (Figure 4A). Nonlinear spatial PL expansion has been reported on monolayer MoS_2: the PL profile becomes broad above the threshold laser power density (∼8.0 kW/cm^2) because EEA enables lower PL QY at higher excitation.[10] Here we note that the incident power ranged up to 10.3 kW/cm^2 in this work, supporting that 0.5% strain leads to EEA suppression. Comparing how the generation rate dependence of diffusion length and PL QY changes with strain, we conclude EEA is the primary driving mechanism behind enhanced diffusion in unstrained counterdoped samples.

To extract the diffusion coefficient of neutral excitons, we use the time-dependent continuity equation for neutral excitons:

$$\frac{\partial n_X(r,t)}{\partial t} = \nabla\cdot[D(n_X)\nabla n_X] + g(r,t) - \frac{n_X}{\tau_X} - C_{EEA}{n_X}^2 \quad (2)$$

where n_X and τ_X are the neutral exciton population density and lifetime, respectively. $D(n_x)$ is the concentration and time-dependent diffusion coefficient for the excitons that reflects both the normal diffusion of excitons and the random faster events triggered by EEA. C_{EEA} is the EEA coefficient. Both the single-exciton lifetime and EEA coefficient are known from the PL QY and lifetime measurements in Figures 1 and 2. At steady state, $\frac{\partial n_X}{\partial t} = 0$. We assume a Gaussian generation rate given by

$$g(r) = g_0 \exp(-2r^2/{w_0}^2) \quad (3)$$

where the peak g_0 is determined by pump intensity and w_0 the pump spot size. To simplify the analysis of each experimental result, we assume that the concentration-dependent diffusion coefficient can be replaced by a constant effective diffusion coefficient, D_{eff}. We numerically solve the differential equation for different generation rates and find an effective diffusion coefficient, D_{eff}, that yields the experimentally measured PL map (comparison in Figures S1 and S2). The extracted D_{eff} is shown in Figure 4B. For an unstrained monolayer, the effective diffusion coefficient increases with generation rate. However, for a strained monolayer D_{eff} is independent of generation rate for 6 orders of magnitude change in pump intensity. At low generation rates D_{eff} increases with strain, possibly due to effective mass change with strain.[15] The effective diffusion coefficient as a function of corresponding PL QY is shown in Figure 4C. An inversely proportional relationship of diffusion coefficient and PL QY is observed for unstrained monolayer WS_2.

The Boltzmann transport equation (BTE) provides a complete description of diffusing excitons while they are recombining through multiple channels, releasing photons and phonons.[26] The momentum and spatial probability distribution of the nonequilibrium exciton gas found by solving BTE have previously been used to explain the interplay between exciton propagation and many-particle interactions in monolayer TMDCs.[5,27,28] To explain our results, here we distill the whole probability distribution into two baths of excitons, hot and cold, that interact with and transform into each other (Figure 4D). Upon absorption of photons and thermalization, cold excitons are created, some of which decay radiatively. Cold excitons are generated at rate G. The excess energy available to a single cold exciton is $E_{ex}-E_{em}$, where E_{ex} is the excitation photon energy and E_{em} is the emission photon energy. In case the EEA channel is active, some excitons relax to the ground state, transferring all its energy (E_{em}) to a nearby exciton. This hot energetic exciton loses its large kinetic energy by diffusing very fast in the crystal in a random direction while emitting phonons. By losing its energy a hot exciton turns into a cold exciton, which can then luminesce. However, if the EEA channel is suppressed, no hot excitons are created. Hot electrons are generated at a rate of $C_{EEA}{n_X}^2$, and each hot electron has an average kinetic energy of E_{em}. The average kinetic energy per exciton $\overline{KE}$ provided to the exciton population in steady state is

$$\overline{KE} \sim \frac{(E_{ex} - E_{em})G + E_{em}C_{EEA}{n_X}^2}{n_X}$$

where the first term indicates the thermal energy from the excitation laser and the second term indicates the energy from the nonradiative recombination of EEA. According to the semiclassical description,[29,30] the diffusion coefficient is determined by the exciton mass M_X and the scattering time τ_s:

https://doi.org/10.1021/acsnano.2c00956
ACS Nano XXXX, XXX, XXX−XXX

$$D_{\text{eff}} = \frac{\tau_s \overline{\text{KE}}}{M_X}$$

By expressing the average kinetic energy as a function of quantum yield (detailed derivation in Supporting Information), one can show that

$$D_{\text{eff}} \sim \frac{E_{\text{ex}}}{\text{QY}} - \frac{E_{\text{em}}}{\text{QY}_0}$$

whereas QY is the quantum yield at any generation rate and QY_0 is the maximum quantum yield at low generation rate. We note that, in Figure 4 (B and C), these simple expressions fit the experimental value very well with only one proportionality factor.

If EEA is active, excitons gain kinetic energy at the nonradiative expense of another exciton (Figure 4D). These hot excitons diffuse fast but lose their energy by releasing phonons. This in turn heats up the lattice, which can be observed in the pump-dependent Raman spectra of monolayer WS_2 (Figure 5). Both E^1_{2g} and A_{1g} peaks of unstrained counterdoped monolayer WS_2 red-shifted with increasing generation rate, whereas the strained monolayer does not show any shift. The lattice temperature of the unstrained monolayer at $G = 5 \times 10^{10}$ cm^{-2} is estimated to increase by 260 °C from the linear temperature dependence of Raman modes with temperature coefficients of -1.25×10^{-2} and -1.49×10^{-2} cm^{-1} K^{-1} for the E^1_{2g} and A_{1g} modes, respectively.[31] Note that changing the crystal temperature in monolayers by heating the substrate does not have the same effect on exciton diffusion, as this process does not create hot excitons at the same energy as EEA (Figure S3).

CONCLUSIONS

In conclusion, we have optically explored neutral exciton transport in monolayer semiconductors at room temperatures. EEA is shown to have a profound effect on exciton propagation, resulting in a strong pump dependence of the measured diffusion drastically different from conventional semiconductors. Our results reveal strain as another tuning knob for mobile optical excitations in 2D materials and show EEA is relevant for the design of optoelectronic devices because it not only affects PL QY but also enhances exciton diffusion.

MATERIALS AND METHODS

Device Fabrication. The flexible devices for optical measurements were fabricated on a polyimide substrate (Kapton, Dupont, 1.5 mm thick). To prevent background PL from polyimide substrate, a metal mirror of Ti (10 nm)/Au (100 nm)/Ti (10 nm) was fabricated using standard photolithography and thermal evaporation, and 50 nm Al_2O_3 was deposited *via* atomic layer deposition (ALD) at 200 °C. WS_2 (HQ Graphene) was mechanically exfoliated on a 50 nm SiO_2/Si substrate. Monolayer WS_2 flakes were picked up with poly(methyl methacrylate) (PMMA) and transferred onto the ALD oxide, followed by a postbaking at 180 °C for 5 min and dichloromethane (DCM) treatment to remove PMMA. As a chemical counterdoping, a 3% Nafion perfluorinated resin solution (Sigma-Aldrich) diluted by ethanol was spin-coated on the prepared monolayer WS_2.[3]

Optical Characterization. PL spectra and QY were measured using a customized micro-PL instrument described in detail in the previous study.[2] An Ar ion laser with a 3 nm line was used as the excitation source. The calibrated PL QY measurement is also described in detail in previous studies.[1,2] A two-point bending method was used to apply a tensile strain in the monolayer WS_2.[32] The nominal applied strain was calculated using the equation $\varepsilon = t/R$, where $2t$ and R are the substrate thickness and curvature radius measured through the cross-section optical image. TRPL measurements were collected using a time-correlated single-photon counting (TCSPC) module. A monochromated line of 514 nm from a supercontinuum laser was used as the excitation source. The 150× objective lens was used to irradiate the sample from the top, and the same lens was used to collect the PL emission from sample. The nominal laser diameter ($1/e^2$ intensity in the Gaussian-shaped spatial distribution) and maximum laser power on the sample were 706 nm and 40.4 μW, respectively, so the maximum power density was approximately 10.3 kW/cm^2. Exciton diffusion images were measured with a fluorescence microscopy setup using the green laser, the same as the excitation source for PL measurement, and a CCD detector (Andor Luca) to acquire images.[4] The samples were excited with a 514.5 nm wavelength laser focused to a diffraction-limited spot. Raman spectra were measured by a Raman microscopic system (Horiba Labram HR Evolution) using an excitation laser of 532 nm.

ASSOCIATED CONTENT

Supporting Information

The Supporting Information is available free of charge at https://pubs.acs.org/doi/10.1021/acsnano.2c00956.

Comparison of experimental PL image and simulated model, temperature effect on PL images with external heating, extraction details of the relationship between diffusion coefficient and PL QY (PDF)

AUTHOR INFORMATION

Corresponding Author

Ali Javey − *Electrical Engineering and Computer Sciences, University of California, Berkeley, California 94720, United States; Materials Sciences Division, Lawrence Berkeley National Laboratory, Berkeley, California 94720, United States;* orcid.org/0000-0001-7214-7931; Email: ajavey@berkeley.edu

Authors

Shiekh Zia Uddin − *Electrical Engineering and Computer Sciences, University of California, Berkeley, California 94720, United States; Materials Sciences Division, Lawrence Berkeley National Laboratory, Berkeley, California 94720, United States;* orcid.org/0000-0002-1265-9940

Naoki Higashitarumizu − *Electrical Engineering and Computer Sciences, University of California, Berkeley, California 94720, United States; Materials Sciences Division, Lawrence Berkeley National Laboratory, Berkeley, California 94720, United States;* orcid.org/0000-0003-3996-6753

Hyungjin Kim − *Electrical Engineering and Computer Sciences, University of California, Berkeley, California 94720, United States; Materials Sciences Division, Lawrence Berkeley National Laboratory, Berkeley, California 94720, United States*

Jun Yi − *NSF Nanoscale Science and Engineering Center, University of California, Berkeley, California 94720, United States*

Xiang Zhang − *NSF Nanoscale Science and Engineering Center, University of California, Berkeley, California 94720, United States; Faculties of Sciences and Engineering, The University of Hong Kong, Hong Kong, China*

Daryl Chrzan − *Materials Sciences Division, Lawrence Berkeley National Laboratory, Berkeley, California 94720, United States; Materials Science and Engineering, University*

https://doi.org/10.1021/acsnano.2c00956
ACS Nano XXXX, XXX, XXX−XXX

of California, Berkeley, Berkeley, California 94720, United States

Complete contact information is available at: https://pubs.acs.org/10.1021/acsnano.2c00956

Author Contributions

#S.Z.U. and N.H. contributed equally.

Author Contributions

S.Z.U., H.K., N.H., and A.J. conceived the idea for the project and designed the experiments. S.Z.U. and N.H. fabricated devices and performed optical measurements. S.Z.U., N.H., and A.J. analyzed the data. J.Y. and X.Z. performed Raman measurements. S.Z.U. and D.C. performed analytical modeling. S.Z.U., N.H., and A.J. wrote the manuscript. All authors discussed the results and commented on the manuscript.

Notes

The authors declare no competing financial interest.

ACKNOWLEDGMENTS

This work was funded by the U.S. Department of Energy, Office of Science, Office of Basic Energy Sciences, Materials Sciences and Engineering Division, under contract no. DE-AC02-05-CH11231 (EMAT program KC1201). N.H. acknowledges support from Postdoctoral Fellowships for Research Abroad of the Japan Society for the Promotion of Science.

REFERENCES

(1) Amani, M.; Lien, D.-H.; Kiriya, D.; Xiao, J.; Azcatl, A.; Noh, J.; Madhvapathy, S. R.; Addou, R.; Kc, S.; Dubey, M.; Cho, K.; Wallace, R. M.; Lee, S.-C.; He, J.-H.; Ager, J. W., 3rd; Zhang, X.; Yablonovitch, E.; Javey, A. Near-Unity Photoluminescence Quantum Yield in MoS□. *Science* **2015**, *350* (6264), 1065−1068.

(2) Lien, D.-H.; Uddin, S. Z.; Yeh, M.; Amani, M.; Kim, H.; Ager, J. W., 3rd; Yablonovitch, E.; Javey, A. Electrical Suppression of All Nonradiative Recombination Pathways in Monolayer Semiconductors. *Science* **2019**, *364* (6439), 468−471.

(3) Uddin, S. Z.; Rabani, E.; Javey, A. Universal Inverse Scaling of Exciton-Exciton Annihilation Coefficient with Exciton Lifetime. *Nano Lett.* **2021**, *21* (1), 424−429.

(4) Kim, H.; Uddin, S. Z.; Higashitarumizu, N.; Rabani, E.; Javey, A. Inhibited Nonradiative Decay at All Exciton Densities in Monolayer Semiconductors. *Science* **2021**, *373* (6553), 448−452.

(5) Kulig, M.; Zipfel, J.; Nagler, P.; Blanter, S.; Schüller, C.; Korn, T.; Paradiso, N.; Glazov, M. M.; Chernikov, A. Exciton Diffusion and Halo Effects in Monolayer Semiconductors. *Phys. Rev. Lett.* **2018**, *120* (20), 207401.

(6) Cadiz, F.; Robert, C.; Courtade, E.; Manca, M.; Martinelli, L.; Taniguchi, T.; Watanabe, K.; Amand, T.; Rowe, A. C. H.; Paget, D.; Urbaszek, B.; Marie, X. Exciton Diffusion in WSe_2 Monolayers Embedded in a van Der Waals Heterostructure. *Appl. Phys. Lett.* **2018**, *112* (15), 152106.

(7) Fu, Y.; He, D.; He, J.; Bian, A.; Zhang, L.; Liu, S.; Wang, Y.; Zhao, H. Effect of Dielectric Environment on Excitonic Dynamics in Monolayer WS_2. *Adv. Mater. Interfaces* **2019**, *6* (23), 1901307.

(8) Zipfel, J.; Kulig, M.; Perea-Causín, R.; Brem, S.; Ziegler, J. D.; Rosati, R.; Taniguchi, T.; Watanabe, K.; Glazov, M. M.; Malic, E.; Chernikov, A. Exciton Diffusion in Monolayer Semiconductors with Suppressed Disorder. *Phys. Rev. B* **2020**, *101* (11), 115430.

(9) Uddin, S. Z.; Kim, H.; Lorenzon, M.; Yeh, M.; Lien, D.-H.; Barnard, E. S.; Htoon, H.; Weber-Bargioni, A.; Javey, A. Neutral Exciton Diffusion in Monolayer MoS_2. *ACS Nano* **2020**, *14* (10), 13433−13440.

(10) Yu, Y.; Yu, Y.; Li, G.; Puretzky, A. A.; Geohegan, D. B.; Cao, L. Giant Enhancement of Exciton Diffusivity in Two-Dimensional Semiconductors. *Sci. Adv.* **2020**, *6* (51), No. eabb4823.

(11) Perea-Causín, R.; Brem, S.; Rosati, R.; Jago, R.; Kulig, M.; Ziegler, J. D.; Zipfel, J.; Chernikov, A.; Malic, E. Exciton Propagation and Halo Formation in Two-Dimensional Materials. *Nano Lett.* **2019**, *19* (10), 7317−7323.

(12) Mouri, S.; Miyauchi, Y.; Toh, M.; Zhao, W.; Eda, G.; Matsuda, K. Nonlinear Photoluminescence in Atomically Thin Layered WSe_2 Arising from Diffusion-Assisted Exciton-Exciton Annihilation. *Phys. Rev. B Condens. Matter* **2014**, *90* (15), 155449.

(13) Cordovilla Leon, D. F.; Li, Z.; Jang, S. W.; Cheng, C.-H.; Deotare, P. B. Exciton Transport in Strained Monolayer WSe_2. *Appl. Phys. Lett.* **2018**, *113* (25), 252101.

(14) Harats, M. G.; Kirchhof, J. N.; Qiao, M.; Greben, K.; Bolotin, K. I. Dynamics and Efficient Conversion of Excitons to Trions in Non-Uniformly Strained Monolayer WS_2. *Nat. Photonics* **2020**, *14* (5), 324−329.

(15) Rosati, R.; Brem, S.; Perea-Causín, R.; Schmidt, R.; Niehues, I.; de Vasconcellos, S. M.; Bratschitsch, R.; Malic, E. Strain-Dependent Exciton Diffusion in Transition Metal Dichalcogenides. *2D Mater.* **2021**, *8* (1), 015030.

(16) Bandić, Z. Z.; Bridger, P. M.; Piquette, E. C.; McGill, T. C. Minority Carrier Diffusion Length and Lifetime in GaN. *Appl. Phys. Lett.* **1998**, *72* (24), 3166−3168.

(17) Wang, F.; Wu, Y.; Hybertsen, M. S.; Heinz, T. F. Auger Recombination of Excitons in One-Dimensional Systems. *Phys. Rev. B Condens. Matter Mater. Phys.* **2006**, *73* (24), 245424.

(18) O'Hara, K. E.; Gullingsrud, J. R.; Wolfe, J. P. Auger Decay of Excitons in Cu_2O. *Phys. Rev. B Condens. Matter* **1999**, *60* (15), 10872−10885.

(19) Deng, S.; Shi, E.; Yuan, L.; Jin, L.; Dou, L.; Huang, L. Long-Range Exciton Transport and Slow Annihilation in Two-Dimensional Hybrid Perovskites. *Nat. Commun.* **2020**, *11* (1), 664.

(20) Paradisanos, I.; Pliatsikas, N.; Patsalas, P.; Fotakis, C.; Kymakis, E.; Kioseoglou, G.; Stratakis, E. Spatial Non-Uniformity in Exfoliated WS_2 Single Layers. *Nanoscale* **2016**, *8* (36), 16197−16203.

(21) Sebastian, A.; Pendurthi, R.; Choudhury, T. H.; Redwing, J. M.; Das, S. Benchmarking Monolayer MoS_2 and WS_2 Field-Effect Transistors. *Nat. Commun.* **2021**, *12* (1), 693.

(22) Kwon, Y.; Kim, K.; Kim, W.; Ryu, S.; Cheong, H. Variation of Photoluminescence Spectral Line Shape of Monolayer WS_2. *Curr. Appl. Phys.* **2018**, *18* (8), 941−945.

(23) Yuan, L.; Huang, L. Exciton Dynamics and Annihilation in WS_2 2D Semiconductors. *Nanoscale* **2015**, *7* (16), 7402−7408.

(24) Pareek, V.; Madéo, J.; Dani, K. M. Ultrafast Control of the Dimensionality of Exciton-Exciton Annihilation in Atomically Thin Black Phosphorus. *Phys. Rev. Lett.* **2020**, *124* (5), 057403.

(25) Akselrod, G. M.; Deotare, P. B.; Thompson, N. J.; Lee, J.; Tisdale, W. A.; Baldo, M. A.; Menon, V. M.; Bulović, V. Visualization of Exciton Transport in Ordered and Disordered Molecular Solids. *Nat. Commun.* **2014**, *5* (1), 3646.

(26) Snoke, D. W. The Quantum Boltzmann Equation in Semiconductor Physics. *Ann. Phys.* **2011**, *523* (1−2), 87−100.

(27) Rosati, R.; Perea-Causín, R.; Brem, S.; Malic, E. Negative Effective Excitonic Diffusion in Monolayer Transition Metal Dichalcogenides. *Nanoscale* **2020**, *12* (1), 356−363.

(28) Perea-Causín, R.; Brem, S.; Malic, E. Phonon-Assisted Exciton Dissociation in Transition Metal Dichalcogenides. *Nanoscale* **2021**, *13* (3), 1884−1892.

(29) Erland, J.; Razbirin, B. S.; Pantke, K.; Lyssenko, V. G.; Hvam, J. M. Exciton Diffusion in CdSe. *Phys. Rev. B Condens. Matter* **1993**, *47* (7), 3582−3587.

(30) Wagner, K.; Zipfel, J.; Rosati, R.; Wietek, E.; Ziegler, J. D.; Brem, S.; Perea-Causín, R.; Taniguchi, T.; Watanabe, K.; Glazov, M. M.; Malic, E.; Chernikov, A. Nonclassical Exciton Diffusion in Monolayer WSe_2. *Phys. Rev. Lett.* **2021**, *127* (7), 076801.

(31) Peimyoo, N.; Shang, J.; Yang, W.; Wang, Y.; Cong, C.; Yu, T. Thermal Conductivity Determination of Suspended Mono- and

Bilayer WS_2 by Raman Spectroscopy. *Nano Res.* **2015**, *8* (4), 1210−1221.
(32) Desai, S. B.; Seol, G.; Kang, J. S.; Fang, H.; Battaglia, C.; Kapadia, R.; Ager, J. W.; Guo, J.; Javey, A. Strain-Induced Indirect to Direct Bandgap Transition in Multilayer WSe_2. *Nano Lett.* **2014**, *14* (8), 4592−4597.

https://doi.org/10.1021/acsnano.2c00956
ACS Nano XXXX, XXX, XXX−XXX